Supplemental Information for

A distributed recurrent network contributes to temporally precise vocalizations

Kosuke Hamaguchi, Masashi Tanaka, and Richard Mooney

Department of Neurobiology Duke University Medical Center

Contents:

Supplemental Experimental Procedures

Temperature manipulations using the Peltier device.

A pair of silver cooling pads made from silver wire (A-M systems, Part #787550, O.D. 381 μm) was attached to one side of Peltier device (CustomThermoelectric, Part #01101-9G30-20CN) and the other side was attached to the custom-made 3D printed water-cooled heat sink made of silver (i.materialize Inc) by using thermo-conductive epoxy (CustomThermoelectric, Part #TE-ASTA-7G). The heat sink was attached to a pair of silicon tubes (A-M systems, Part #8061) to perfuse water through the water channel in the heat sink (~450 μl/min). The cooling pads were shaped to fit the lateral-medial distance of HVC (4.8 mm) or Uva (2.4 mm, targeting the medial edge of Uva to avoid damage). For Uva cooling, polyimide tubing (MicroLumen, Inc. #315-I.5, O.D. 873 μm) was also attached to the probes as an insulator to enhance the heat delivery. In a subset of experiments, an extended heat sink was placed on the lower leaflet of the skull to limit temperature changes in HVC caused by the cooling probe implanted in Uva. Birds were anesthetized with 1.5–2% isoflurane in oxygen and placed in a stereotaxic apparatus. The position of HVC was stereotaxically determined (0.0 mm anterior, 2.4 mm lateral from the bifurcation of Y-sinus). The position of Uva was determined with reference to the auditory thalamic nucleus Ovoidalis (Ov; 2.8 mm anterior, 1.0 mm lateral from Y-sinus, 4.5 – 5.0 mm deep), which was identified by its robust auditory responses. Uva was located at 1.5-1.7 mm posterior, 0.5 mm lateral of Ov. The outer layer of skull over the target region was largely removed and the inner layer of skull was removed to create an opening slightly larger than the size of the cooling pads. For HVC cooling, the cooling pads were placed over the dura. For Uva cooling, a column of brain tissue 4.0 mm deep was removed by aspiration and the probes were inserted near the medial-dorsal side of Uva (300 – 800 μm, Figure S4). The surface of the brain was covered with Kwik-Kast (WPI, Inc), and the extended legs of the heat sink were cemented to the skull. The temperature of the target region was measured by a thermocouple (Omega, Part #5SRTC-TT-K-40-36) at the end of the experiment while the birds were anesthetized under Isoflurane (1.0% in Oxygen). For Uva cooling, retrograde tracer (Molecular Probes, Dextran Alexa Fluor 488, 10,000 MW) was injected in HVC either before or after the experiments to histologically identify Uva. The temperature change ΔT is defined as the relative difference from the physiologically normal brain temperature (~40 Celsius), which was maintained by running the Peltier device in the slightly warming direction to offset the cooling effect of placing the probe on the surface of the brain (Figure S1F, H). Song timing effects were measured as the relative changes from this “normal” temperature condition.

Intracellular recordings in singing birds.

The intracellular microdrive (original design by M. Fee (Long et al., 2010)) was built with a 3D printed plastic base and chassis (Agile Manufacturing, Inc, Ontario, Canada). A miniaturized headstage (by I. Yoon, equivalent to HS-2A headstage with gain x0.1, Axon Instruments) was mounted on the back of the base to amplify signals and receive command current from the intracellular recording amplifier (AxoClamp-2B, Axon Instruments) through a flexible tether cable (Omnetics, MN, USA). A linear actuator (Part # 0206A001B+02/1 47:1-Y2825, Micromo, FL, USA) controlled the position of the depth of the sharp microelectode. The microdrive was surgically implanted over the right HVC using stereotaxic coordinates (2.4 mm lateral, 0 mm anterior from Y-sinus). HVC_{RA} neurons were identified by antidromic stimulation with a bipolar stimulating electrode (a pair of 75 μm diameter silver wires, ~500 μm apart, A-M systems, WA, USA) implanted in RA. HVC_X neurons were identified by their spontaneous, DC-evoked, and singing-related activity. In total, we recorded from n = 24 identified HVC_{RA} neurons and n = 82 HVC_X neurons. Recordings were attempted for approximately 7-21 days per bird and recording microelectrodes were replaced maximally three times a day. Signals were recorded with in-house software written by KH in MATLAB (Mathworks).

Synaptic event analysis in singing birds. To detect depolarizing synaptic events during singing, an algorithm detecting large deviations of dV/dt was used (Ankri et al., 1994)(see example traces in Figure S7A, B). To align synaptic event data to the song, we identified the most typical syllable sequence using a semi-automatic algorithm run by a support vector machine as described below (see Syllable and gap duration analysis). The mean onset timings of identified syllables were defined as the standard timing markers. Detected synaptic events during a specific syllable sequence were aligned to each sound onset and linearly displaced relative to the standard timing markers. Then, synaptic event rates for a given cell were calculated as across trial-averages of synaptic events smoothed by a Gaussian filter (3ms SD). The time stretch was usually within 0 – 20 ms range. The signal correlation between cells was calculated as the correlation coefficient of the trial-averaged synaptic event rate within the typical syllable sequence. Surrogate data were generated by randomly shuffling the position of dPSP timings. This procedure was repeated to yield 10,000 pairs of shuffled data, and the p-value was calculated from the distribution of correlation coefficients generated from the shuffled data. The power spectrum of dPSPs of each cell was calculated by the multi-taper spectrogram of detrended, trial averaged dPSP rate (DPSS bandwidth parameter 4, number of tapers = 3).

Brain slices. After induction of inhalation anesthesia (isoflurene), the bird was decapitated, and the brain was removed rapidly and placed in oxygenated ice-cold artificial CSF (ACSF). The ACSF consisted of (in mM) 119 NaCl, 2.5 KCl, 1.3 $MgCl_2$, 2.5 $CaCl_2$, 1 NaH_2PO_4, 26.2 $NaHCO_3$, and 11 glucose, equilibrated with 95%O_2/5%CO_2. Equiosmolar sucrose and $CaCl_2$ were respectively substituted for NaCl

and $MgCl_2$ during the tissue preparation stage. Sagittal brain slices that included HVC were cut at 300 μm thickness and transferred to a holding chamber (37 ^{o}C) for 30 mins and maintained in room temperature until use.

Excitatory post-synaptic current (EPSC) and Calcium current recordings. For EPSP onsets and I_{Ca} rise time recordings, we made targeted patch-clamp recordings using MultiClamp 700B (Molecular devices) and pClamp software. Recordings were performed in 20 μM BMI with Cs-based intracellular solution (130 Cs-methanesulfonate, 10 HEPES, 0.2 EGTA, 4 ATP-Mg, 0.3 GTP-Na_3, 10 phosphocreatine-Na_2, 8 TEA-Cl, 5 QX-314-Br, and 0.05 Alexa 594 hydrazide (pH 7.3, adjusted with CsOH; 295 mOsm), in mM). Electrodes were made with borosilicate glass pipettes (Patch, O.D. 1.5 mm, I.D. 0.86 mm, Sutter Instruments) pulled to 5-8M ohm when filled with Cs-based internal solution. For EPSC recordings, a bipolar stimulating electrode was placed in the fiber tract caudal to HVC to evoke EPSCs in HVC_{RA} neurons. Latency to EPSC onsets was detected as the time of peak of smoothed dI/dt (box filter was applied with a window of 5 data points [0.25 ms]) from the stimulus onset. Calcium currents were activated by depolarizing HVC_{RA} neurons to -30 mV for 500 ms from the resting membrane potential of -90 mV to fully activate calcium channels. Rise time was detected as the time of the peak of the calcium current from the current onset, determined by the peak of smoothed dI/dt (box filter was applied with a window of 5 data points [0.25 ms]). Calculation of Q_{10} was based on 2 data points with min and max temperature (32-38 or 30-38 ^{o}C). The direction of temperature changes was counterbalanced to exclude the effects of rundown of calcium currents. Cells that exhibited substantial rundown during recording or resting current of < -100 pA with the holding potential of -70 mV were excluded from the analysis.

HVC paired recordings. The details of the paired recordings from HVC slices were fully described in (Mooney and Prather, 2005). Briefly, for the measurement of local synaptic latency, we made sharp intracellular recordings using AxoClamp2B amplifier (Molecular devices) and a custom data acquisition program (Labview, National Instruments). Electrodes were made with borosilicate glass pipettes (O.D. 1.0 mm, I.D. 0.5mm, Sutter Instruments, Novato, CA) pulled to form 80-120M ohm resistance when filled with 2M potassium acetate. In paired recordings, one or two action potentials were elicited in turn from each neuron in the pair by passing brief (~10 ms) depolarizing current pulses (0.5 to 1 nA) through the recording electrode while monitoring the other cell for evoked PSPs. The bath temperature was changed (range from 23 ^{o}C to 37 ^{o}C, average $\Delta T = 5.9$) to measure the temperature sensitivity of the synaptic latencies. A subset of data was also obtained from the targeted patch-clamp recording method described above, using Potassium-based internal solution (124 K-gluconate, 4 NaCl, 10 HEPES, 2 EGTA, 2 $MgCl_2$, 2 ATP-Mg, 0.3 GTP-Na_3, 10 phosphocreatine-Na_2, and 0.05 Alexa 594 hydrazide (pH 7.3,

adjusted with KOH; 295 mOsm), in mM). The action potential onset was defined as threshold crossing event of the membrane potential (~20mV from baseline). The max dV/dt was used to detect synaptic onset. Two data points were used to estimate Q_{10}.

Table S1: Stability of Q_{10} values

One potential concern is the extent to which the propagation of neural activity and song timing are well characterized by Q_{10} values, which is a necessary precondition to compare Q_{10} values computed for brain and behavior. Specifically, we note that using Q_{10} ($L1/L2 = Q_{10}^{(T2-T1)/10}$) values to characterize temperature effects implicitly assumes that the ratio of time constant changes only depends on the temperature difference $\Delta T = T2-T1$ and not on the on absolute temperature T2 and T1. To confirm the independence of Q_{10} values within the range of temperatures studied here, we calculated Q_{10} values from maximal temperature differences ($\Delta T<-6\ ^{o}C$; from ~40 ^{o}C to less than ~34 ^{o}C) and intermediate temperature differences ($-6\ ^{o}C <= \Delta T < -3\ ^{o}C$; from ~40 ^{o}C to more than 34 ^{o}C). These calculations confirmed that Q10 values measured for song timing did not differ between the intermediate and maximum temperature ranges (Table S1). Similar calculations confirmed that the Q_{10} values of both synaptic and action potential latencies measured for activity propagation times within HVC (data in Figure 2) and across the recurrent network (data in Figure 3) did not differ between the intermediate and maximum temperature ranges. These analyses confirmed that temperature effects on song timing and the propagation of neural activity within the finch's brain are well characterized by Q10 values.

	Syllable and gap Q_{10} (n=23)	Local latencies; synaptic Q_{10} (Orthodromically evoked AP Q_{10})	Network latency (synaptic + AP) Q_{10}
Q_{10} estimated from $\Delta T < -6\ ^{o}C$ (used in the main text).	1.27 ± 0.03	2.5 ± 0.3 (2.01 ± 0.22)	1.25 ± 0.15
↑ p-value ↓	P=0.23	P=0.3 (P=0.08)	P = 0.95
Q10 estimated from middle range $-6 <= \Delta T <-3$	1.21 ± 0.03	2.1 ± 0.3 (3.7 ± 0.9)	1.26 ± 0.07

Table S1 (related to Figure 2) | Q10 values do not depend on temperature ranges. mean ± SEM.

Simulation Methods

To understand the fundamental differences in synaptic activity patterns generated by local and distributed synfire chains, we constructed computational models of two types of chain networks that relied on minimal assumptions. Following experimental observations (Hahnloser et al., 2002; Long et al., 2010), we set the following constraints to the models: i) ~50% of HVC_{RA} neurons generate action potentials during singing; ii) synaptic activity is non-zero outside of action potential timings; iii) the onset timing of synaptic inputs and the timings of action potentials are precise between motifs (or runs of simulations). We simulated network activity in each model and measured the timing of synaptic activity patterns in randomly selected pairs of neurons. These simulated recordings revealed that pairs of neurons in the local chain model exhibit no correlated synaptic activity whereas neurons in the distributed chain model display significant correlations in their synaptic activity.

Local chain model

We consider a local chain model consisting of 100 timing nodes embedded in a randomly connected network (Figure S6A). Under the assumption that a synchronized action potential activity takes ~5 ms to travel from one node to the next in the chain, this network will generate ~500 ms of sequential activity, which roughly corresponds to the duration of a zebra finch song motif. A set of excitatory neurons are randomly selected with a probability *F* to represent one timing node, and connected to the other randomly selected excitatory neurons representing the next timing. The connection from *j*-th neuron in *l-1* th node to *i*-th neuron in *l*-th node, $J_{ij}^{l}J_{ij}^{l}$ is defined by the Hebbian learning rule;

$$J_{ij}^{l} = \xi_i^l \xi_j^{l-1} J_{ij}^{l} = \xi_i^l \xi_j^{l-1},$$

where $\xi_i^l = \{0,1\} \xi_i^l = \{0,1\}$ is the silent/activated state of *i*-th neuron in the *l*-th node. The vector $\xi^l = [\xi_1^l, \xi_2^l, \ldots, \xi_N^l]\, \xi^l = [\xi_1^l, \xi_2^l, \ldots, \xi_N^l]$ is called a memory pattern of *l*-th layer. The feedforward network embedded with sparse memory patterns have stable states in which synchronized action potentials propagate over multiple layers (Ishibashi et al., 2006). Because previous experiments reported that a small subset of HVC_{RA} neurons could fire multiple times during a single motif in zebra finches (Hahnloser et al., 2002; Long et al., 2010), the neuron once selected is not excluded from a later selection process, with the consequence that one neuron could be involved in more than one timing representation in the motif. Following experimental observations that nearly half of HVC_{RA} are active during song (Hahnloser et al., 2002), we set $F = 1-(0.5)^{1/P} \sim 0.0069$ in the local chain model.

We define the critical synaptic strength $J_c J_c$ such that the membrane potential reaches the action potential threshold under the condition that the activity pattern of the presynaptic layer completely overlaps with the memory pattern (the inner product of the memory pattern and activity vector is 1; $1/N\sum_i^N \xi_i^l x_i^l = 1$

$1/N\sum_i^N \xi_i^l x_i^l = 1$ where $x^l = [x_1^l, x_2^l, \dots, x_N^l]$ $x^l = [x_1^l, x_2^l, \dots, x_N^l]$ is the population activity vector of *l*-th layer). Synaptic connection strength J is set to 10 % larger than J_c.

Recurrent local interactions were modeled by adding a population of 1000 inhibitory HVC_I neurons which make the ratio of the number of inhibitory to excitatory neurons 1:4. The number of presynaptic excitatory (HVC_{RA}) neurons for one postsynaptic neuron is C_E C_E and the number of presynaptic inhibitory neurons (HVC_I) for one neuron is $\beta C_E \beta C_E$ where $\beta\beta$ is the ratio of the number of inhibitory to excitatory neurons ($\beta = \frac{1}{4} \beta = \frac{1}{4}$). Here, we set $C_E = 40 C_E = 40$ which gives a random connection probability of 0.01 (except for Figure S6I). The synaptic strength is set to J J_c for excitatory synapses and $-gJ J_c - g J_{th}$ for inhibitory synapses. The parameter gg represents the ratio of inhibitory to excitatory synapse strength. When the firing rates of excitatory and inhibitory neurons are the same, $g = \frac{1}{\beta} = 4$ $g = \frac{1}{\beta} = 4$ gives the exact balance of inputs from random-recurrent connections. We set the network state g = 5 (i.e., slightly inhibitory dominant) to prevent unstable oscillatory states (Brunel, 2000). The other HVC projection neuron type (i.e., the HVC_X cell) is not necessary for singing (Scharff et al., 2000), therefore we did not explicitly model HVC_X cell activity here.

Distributed chain model

We consider a distributed chain model that consists of four groups of neurons representing four song production nuclei: HVC, RA, the brainstem vocal respiratory group (VRG), and Uva, a major afferent to HVC that links the VRG to HVC and that is critical to singing (Figure S6E). Each group consists of 1600 excitatory neurons and 400 inhibitory neurons. For each group, a set of excitatory neurons is randomly selected with a probability *F* to represent one timing node. The neurons in a node are assigned as the activated neurons and make long-range connections to the activated neurons in the next timing node in the next group following the Hebbian learning rule. Similar to the local chain model, selected neurons are not excluded from the later selection process. Neurons in the fourth group (i.e., Uva) make long-range connections to neurons in the first group (HVC) to form the circular chain structure. This process is repeated P times to generate a longer chain structure embedded in the distributed network. We set P = 25 so that activity propagates in total through 100 nodes in the distributed chain model (25 cycles in total). This 100-layer distributed network generates ~500 ms of sequential activity, which roughly corresponds to the duration of a zebra finch song motif with the assumption that a synchronized action potential volley takes ~5 ms to travel from one node to the next. Therefore, the connection from *j*-th neuron in *l-1* th node to *i*-th neuron in *l*-th node, $J_{ij}^l J_{ij}^l$, is defined as follows;

$J_{ij}^{l} = \sum_{k}^{P} \xi_i^{(l,k)} \xi_j^{(l-1,k)} J_{ij}^{l} = \sum_{k}^{P} \xi_i^{(l,k)} \xi_j^{(l-1,k)}$,

where $\xi_i^{(l,k)} = \{0,1\} \xi_i^{(l,k)} = \{0,1\}$ is the *k*-th silent/active state of *i*-th neuron in *l*-th node. The vector $\xi^{(l,k)} = \left[\xi_1^{(l,k)}, \xi_2^{(l,k)}, \ldots, \xi_N^{(l,k)}\right] \xi^{(l,k)} = \left[\xi_1^{(l,k)}, \xi_2^{(l,k)}, \ldots, \xi_N^{(l,k)}\right]$ is called *k*-th memory pattern of *l*-th layer. Following experimental observations that nearly half of HVC_{RA} are active at least once during song (Hahnloser et al., 2002), we set $F = 1 - (0.5)^{\frac{1}{P}} \sim 0.0273 F = 1 - (0.5)^{\frac{1}{P}} \sim 0.0273$ which will result in action potential activity in ~50% of the HVC_{RA} neurons over a ~500 ms period. This indicates that less than 3 % of neurons are active at one time in one group, but within a single run of activity, approximately 50 % of neurons will be activated. Synaptic connection strength is set to 10 % larger than $J_c J_c$. Random local connections are generated exactly in the same manner as we described in the local chain model.

Note that the focus of this modeling effort is to understand whether differences in the connectivity of HVC neurons play an important role in defining the correlation level of synaptic input patterns, regardless of the implementation of the dynamics of the RA and VRG groups. The only assumption we make here is that the RA and VRG groups can rapidly convey changes in the HVC group's firing rate back to HVC during singing. Therefore, the implementation of local network structure in each group is statistically similar in the distributed chain model.

Neuron model

To understand the relationship between the synaptic input distribution and network activity patterns without involving the details of the implementation of action potential generation, we used the leaky integrate-and-fire neuron model to implement the membrane dynamics of the HVC_{RA} and HVC_I neurons using the same model parameters. The membrane potential dynamics of a neuron are described as:

$$\tau_m \frac{dv_i}{dt} = -(v_i - V_L) + I_i,$$

$$\tau_s \frac{dI_i}{dt} = -I_i + \tau_s \sum_j J_{ij} \sum_k \delta(t - t_j^k - D),$$

where $v_i v_i$ is the membrane potential of the *i*-th neuron, $V_L V_L$ is the leak potential, and $I_i I_i$ is the input current of *i*-th neuron. $\tau_m \tau_m$, $\tau_s \tau_s$ are the membrane and current time constant, respectively. $\delta(t) \delta(t)$ is the delta-function, and $t_j^k t_j^k$ is the *k*-th action potential timings of *j*-th neuron, DD is the delay between the timing of presynaptic action potential to the postsynaptic synaptic onset. When the membrane potential exceeds the threshold voltage $V_{th} V_{th}$ ($v_i > V_{th} v_i > V_{th}$), a neuron emits an action potential and the membrane potential is set to the reset potential $V_{reset} V_{reset}$ and remains insensitive to the input current during the refractory time period $t_{ref} t_{ref}$. The parameters of the model and networks are summarized at

the end of this section. We did not incorporate bursting properties in individual HVC_{RA} neurons to reduce the complexity of the model. This should not affect synaptic activity patterns because the membrane potential time constant (~20ms) is slow relative to the firing rate within the burst (>200Hz); this slow time constant will filter out higher frequency components of the synaptic activity driven by high frequency action potential bursts.

Behaviors of local and distributed chain models

The architecture of the network plays an important role in shaping synaptic correlations. In local chain models, the action potential activity traveling through the local chain model is temporally uniform. The resultant synaptic activity patterns transmitted by these random local connections are also temporally random and uncorrelated between neurons. In contrast, in the distributed chain model, synaptic inputs are transiently generated in many neurons once in every four propagation steps, while the rest of the time synaptic input would remain relatively silent. The temporal organization of active and silent phases of synaptic activity, which contrasts with the uniform synaptic activity of the local chain model, could generate detectable correlations between neurons within HVC. We confirmed these predictions using simulations of the local and distributed chain models.

Simulations of neural activity in local and distributed chain models

First, the simulation of a local chain model (Figure 6F, Figure S6A) displayed sequential action potential activity that propagated through 100 groups in a stable manner. To quantify the similarity of activated patterns to the embedded patterns, we calculated the overlap parameters. The overlap parameters are defined as the inner product of the population activity vector and each memorized pattern. An overlap parameter is 0 when the activated pattern is orthogonal to the memory pattern and 1 when all the neurons in the memory pattern are activated. The overlap parameters showed sequential activation patterns and approached a value of 1 (Figure S6B,C), suggesting that the embedded patterns are activated in the learned order. Then, we randomly sampled the membrane potential activity of 20 excitatory neurons (Figure 6G). Examples of membrane potential traces from 2 runs of simulations are shown (Figure S6D). The baseline synaptic activity was non-zero and within a cell was stereotyped between runs, as we observed in the intracellular recordings experiments made in the HVC of singing finches. However, no significant correlation was detected in synaptic onset timings between pairs of neurons, as revealed by the correlation coefficient analysis (Figure 6I, Top, gray circles). Still, it is possible that weak synaptic correlations could be detected by measuring the population average. Therefore, we calculated the population averaged synaptic activity from half of the neurons in the group but this average activity diverged from that calculated using the other half of the neurons in the population (Figure 6I, Bottom,

gray circles). These results suggest that synaptic input timings in different neurons are not correlated in a local chain model.

Second, we simulated the distributed chain model (Figure 6A, Figure S6E), in which sequential action potential activity propagates through the four groups repeatedly (i.e., 25 cycles). To clearly visualize the sequential action potential activity patterns, we calculated overlaps parameters of the first (i.e., the HVC) group. The overlap parameters showed stable transitions of action potential activity from the first to the last memorized patterns (Figure S6F,G), indicating that divergent connections embedded in the system did not prevent stable transitions. However, when one of the overlap parameters is activated, some of other overlap parameters are also active which is evident from the small baseline fluctuations of other overlap parameters (Figure S6F,G). Next, we randomly sampled 20 excitatory neurons activity from the HVC group (Figure 6C). Although the action potential activity in different cells formed a sequential pattern, underlying synaptic activity appeared to be both more frequent and correlated between cells. Examples of membrane potential traces from 2 runs of simulations are shown in Figure S6H. Neurons in the distributed chain model have frequent incidents of correlated synaptic onsets (highlighted by dashed lines, Figure S6H). In fact, the correlations in the synaptic onset timings between pairs of neurons were significant (Figure S6I, Top, red circles). Furthermore, the population averaged synaptic activity from half of neurons in the group had clear similarities to that calculated from the other half (Figure S6I, Bottom, red circles).

Both our local and distributed models also captured the observation made with extracellular and intracellular recordings in singing birds that a small fraction of HVC_{RA} neurons can be active more than once in the motif (see Figure 2b, neuron #2, of Hahnloser et al., 2002; Supplementary Figure 2, Bird#15 of Long et al., 2010). The percentage of neurons active more than once in our simulations is ~13% (see following section for an accounting of this percentage); the actual percentage of HVC_{RA} neurons that are of this less sparsely active type is unknown. To summarize, our simulation results indicate that neurons within a single group in the distributed chain model exhibit significantly correlated synaptic inputs, whereas neurons in the conventional local chain model do not exhibit correlations in their synaptic activity patterns (Fig. 6I). Furthermore, this prediction is highly robust in the face of variations in network structure within the range of parameters where sequential activity propagates in a stable manner (Figure S6I). For example, we can change the balance of random local interaction and feedforward interaction. The parameter $C_E C_E$ defines the number of presynaptic excitatory neurons. The number of Inhibitory neurons is defined as $\beta C_E \beta C_E$, therefore excitatory-inhibitory balance is maintained. One reasonable expectation of a local chain model is that neurons should display higher synaptic correlation levels if the

number of local connections (C_E) is changed. However, we found that changing C_E did not change the correlation level of local chain models (Figure S6I) until the network attained a new stable state where neurons maintain random action potential activity through local random connections (Figure S6J,K). The transition from sequential to random activity states can induce correlations in the system (Figure S6I), but such a network no longer has HVC-like stable sparse sequential action potential activity.

Synaptic Correlation Analysis in Simulations

Synaptic correlation is calculated as the correlation coefficient of trial-averaged synaptic event rates between pairs of neurons. The trial-averaged synaptic event rates were obtained by averaging 5 runs of simulations. Ten randomly selected pairs of excitatory neurons from the local chain model or from the HVC group in the distributed chain were used for this analysis. We repeated this procedure in 5 different realizations of network architecture, which were generated from different seeds of pseudo-random variables to calculate the synaptic correlations. The similarity of the population averaged synaptic event rate was calculated as the correlation coefficient of population averaged synaptic activity obtained from two groups neurons, each containing 10 neurons. Data were generated in the same way as described above, using 5 runs of simulations repeated with 5 different network realizations.

Overlap Analysis

Overlaps between the action potential activity and *k*-th memorized patterns are defined as:

$$m^k(t) = \frac{1}{N}\sum_i^N \xi_i^k x_i(t) m^k(t) = \frac{1}{N}\sum_i^N \xi_i^k x_i(t),$$

where $x_i(t) = 1 x_i(t) = 1$ if neuron *i* generates an action potential at time *t*, otherwise set to zero. We smoothed $m^k(t) m^k(t)$ with 1ms SD Gaussian window to account for the jitter in action potential timings in each trial. The lower and upper bound of the overlap parameter is zero (no overlap with the memory pattern *k*) and 1 (complete overlap with the memory pattern *k*).

Linearity Index

Whether memorized patterns are sequentially activated in the correct order was quantified by calculating a linearity index, which was defined as:

$$Lin = \frac{\#\text{ of correct transitions}}{\#\text{ of total transitions}}$$

For example, if the memory pattern is embedded in the order of [1,2,3,4,5], then an activation pattern [1,2,4,5] has *Lin* = 2/3. This index is 1 when only the correct transitions are observed and 0 when no

correct transitions are observed. Activation of a pattern is detected as the threshold exceeding events of overlap parameters. Here, the threshold is set to 0.3.

Expected ratio of active cells

We consider the problem of selecting cells with a probability F for multiple times (N) with replacement. This means a cell can be selected more than once. The probability of a cell k-times selected among N-times selection process is described as the binomial distribution,

$P(N,k) = {}_NC_k\, F^k\, (1-F)^{(N-k),}$

where ${}_NC_k = N! / ((N-k)!\, k!)$.

From the experimental constraint that nearly half of cells do not fire action potential during singing, we can calculate $F = 1-(0.5)^{1/N}$.

For the local chain model, we have N=100 layers of propagation steps, therefore F = 0.0069.

Next, the probability that a cell fires once is

P(N,1)= N * F * (1-F)N-1 = 0.3478.

The remaining is the probability that a cell fires more than once, which is 0.1522. For a circular chain model, N = 25, then F = 0.0273 and the probability of a cell fire more than once is 0.1486. For a finite size simulation, there is a small fluctuation from this value (in our simulation, both models are ~0.13).

Summary of the network and neuron model parameters.

Network parameters	In equation	Unit	Local chain	Distributed chain
Connection strength (excitatory) [1]	J	J_c *	1.1	1.1
Number of local excitatory presynaptic neurons [2]	C_E		40	40
Ratio of number of Inh/Exc neurons	β		1/4	1/4
Number of local inhibitory presynaptic neurons	βC_E		10	10
Ratio of the strength of Inh/Exc synapse	g		5	5
Connection strength (inhibitory)	$-gJ$	J_c	-4.4	-4.4
Number of regions			1	4
Number of excitatory neurons in one region			4000	1000
Number of memorized patterns in HVC	P		100	25
Memory pattern firing rate	F		0.0069	0.0273

1) J_c is defined as the critical strength of synaptic efficacy that drives the membrane potential reach to the action potential threshold when a complete memory pattern is activated in the presynaptic neurons.

2) C_E is varied in Figure S6 to test the robustness of the model.

Single neuron parameters		Unit	Value
Membrane time constant	τ_m	ms	20
Synaptic exponential decay time constant	τ_s	ms	2
Leak potential	V_L	mV	-60
Threshold potential	V_{th}	mV	-50
Reset potential	V_{reset}	mV	-60
Refractoriness	t_{ref}	ms	2
Synaptic delay	D	ms	4

3. Supplemental Figures

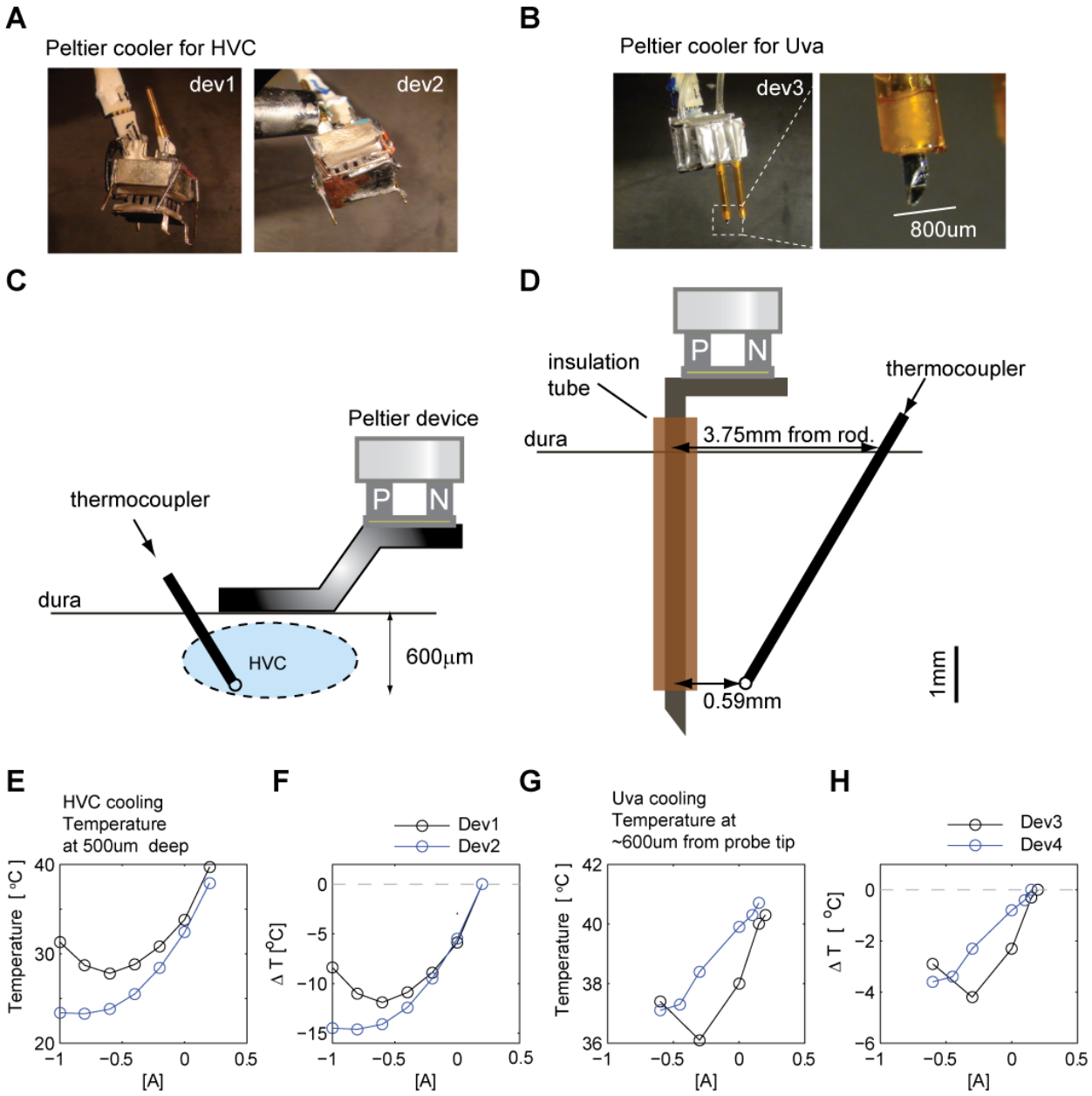

Figure S1 (related to Figure 1)| Custom made Peltier cooling devices for surface and deep cooling. **A,B,** Peltier cooling devices for HVC surface cooling (A) and Uva cooling (B). **C,D,** Schematic diagram showing the methods to measure temperature in HVC (C) and near Uva (D). **E,F,** Typical brain temperature for a given current (E). Even without applying current, we observed that placing a metal plate coupled to a heat sink significantly cools the brain by ~ 2 °C, as also reported in (Long and Fee, 2008). Therefore, we compensated for this cooling offset by slightly warming the brain. The change of brain temperature was measured relative to this compensated (warmed) temperature (F). Temperature was measured at least 30 sec after the current setting was changed. **G,H,** Similar measurements made ~5 mm deep in the brain close to Uva. Compared to the HVC surface cooling probe, the Uva cooling probe has less cooling capacity at the tip because of the larger surface area along the probe's length.

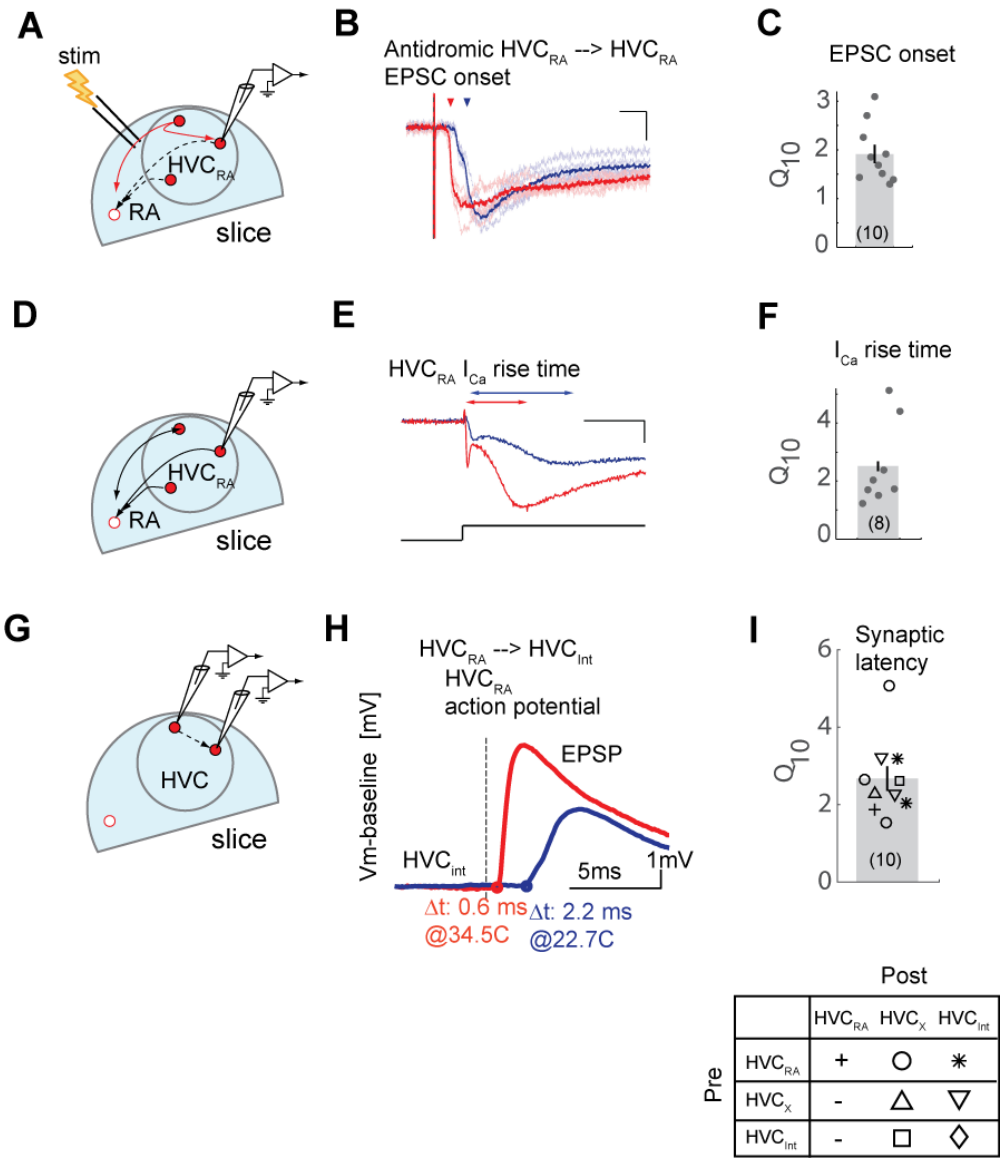

Figure S2 (related to Figure 2) | A, Schematic diagram of the experimental setup to measure local HVC_{RA} - HVC_{RA} interactions in brain slices. **B**, An example of an EPSC evoked in an HVC_{RA} cell by antidromic stimulation of HVC_{RA} axons. (red: 38 °C, blue: 32 °C). Scale bar: 5 ms, 50 pA. **C**, Bath temperature significantly affects synaptic transmission between HVC_{RA} neurons (n = 10 cells, Synaptic onset latencies Q_{10} = 1.91 ± 0.19). **D**, Schematic diagram of the experimental setup to measure voltage dependent Ca currents HVC_{RA} cells in brain slices. **E**, An example of the Ca current evoked in an HVC_{RA} cell (red: 38°C, blue: 32 °C). Command voltage is from -90 mV to -30 mV; recordings were performed with cesium and QX-314 in the pipette to block potassium and sodium currents. Scale bar: 5 ms, 200 pA. **F**, Bath temperature significantly affects the rise time of I_{Ca} in HVC_{RA} cells (n = 9 cells, Q_{10} = 2.51 ± 0.51). **G**, Schematic diagram of paired sharp/patch recordings in HVC slices to measure the latencies of synaptic transmission within HVC. **H**, An example of EPSP recorded in HVC_{Int} evoked by an action potential in an HVC_{RA} cell. **I**, Bath temperature significantly affects synaptic transmission between different HVC PN types and interneurons (n = 10 pairs, Q_{10} = 2.67 ± 0.31). Mean ± SE.

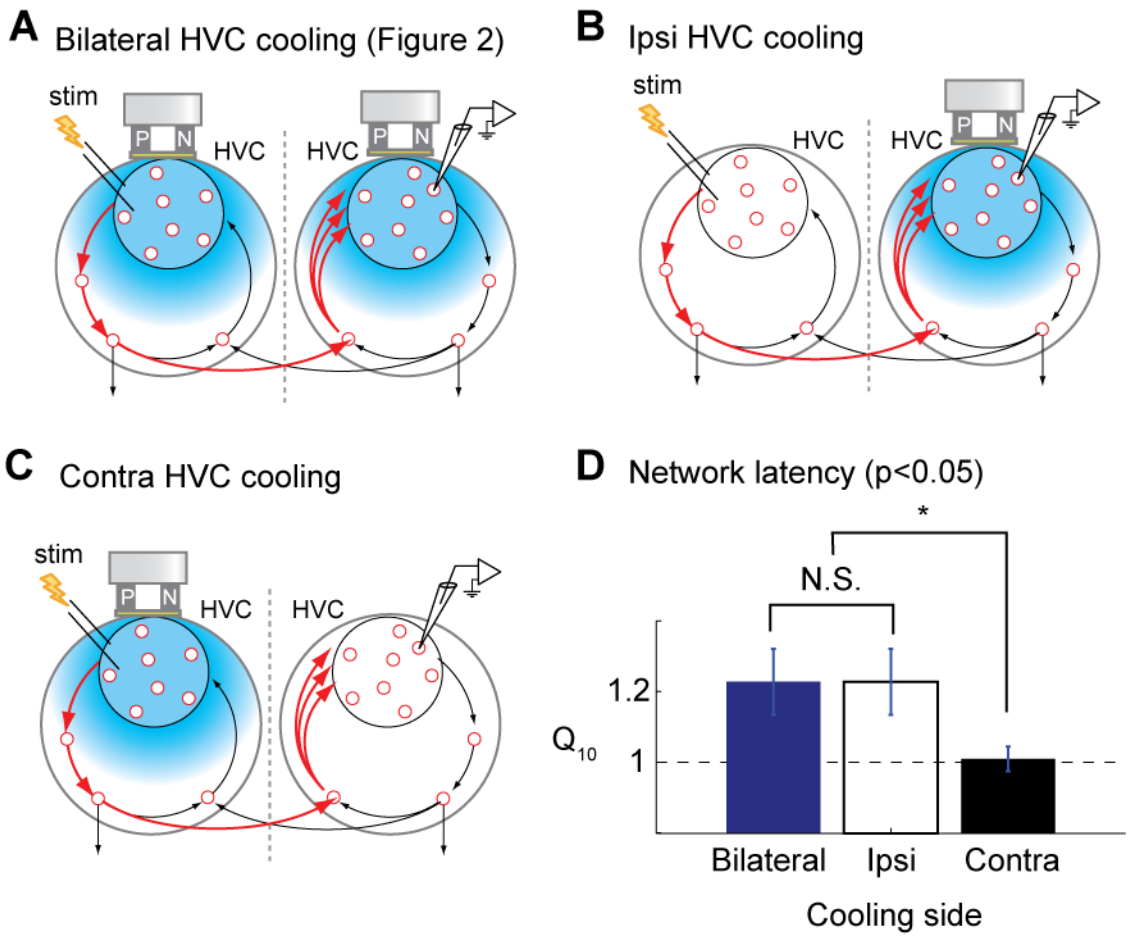

Figure S3 (related to Figure 3) | Dilation of activity propagation is largely attributable to temperature effects on synaptic transmission, as changes in axonal conduction times were negligible. A-C, Schematic diagrams of the experimental setup to compare the effect of (A) bilateral, (B) ipsilateral, (C) contralateral HVC temperature manipulations. **D**, Temperature manipulation of HVC on the stimulating side (contra) had no significant effect on the synaptic onset and action potential timings (n = 7, Q_{10} = 1.01 ± 0.03; no significant difference from Q_{10} = 1; P=0.82). The lack of an effect of contralateral cooling on activity propagation suggests that focal cooling of HVC exerts negligible effects on axonal conduction velocity near the cooled site. In contrast, temperature manipulation on the side of the intracellular recording exerted effects on activity propagation through the recurrent network similar to the effects of bilateral HVC cooling (Ipsi; n = 4, Q_{10} = 1.23 ± 0.09; no significant difference from bilateral cooling effect, n = 18, Q_{10} = 1.21 ± 0.04, P=0.85). This result suggests that the delayed synaptic response observed in bilateral HVC cooling is largely attributable to effects on synaptic transmission local to the recorded cell.

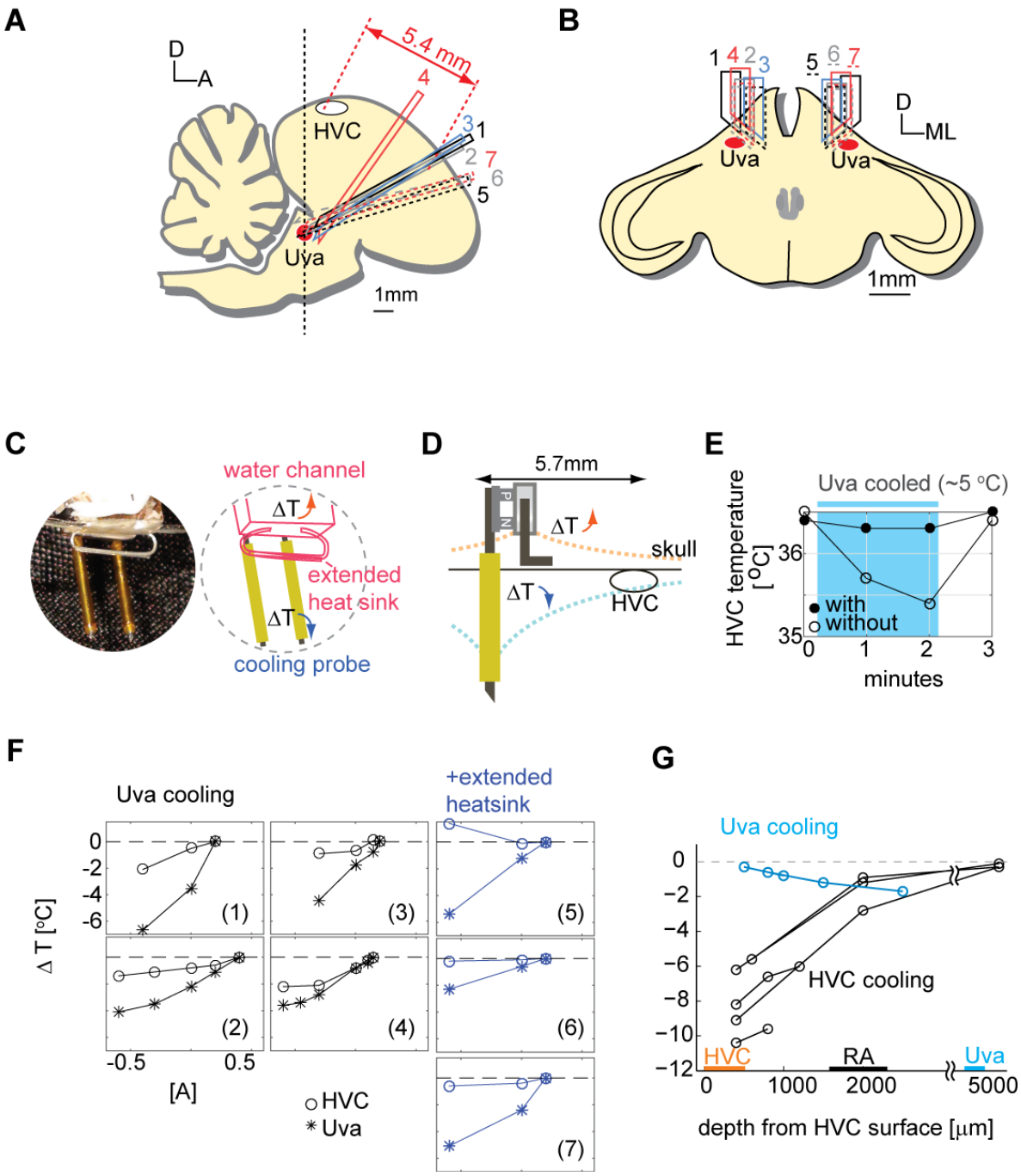

Figure S4 (related to Figure 4) | Locations of cooling probes used in deep brain temperature manipulations. A,B, Reconstructed positions of the cooling probes in four birds used for deep brain cooling experiments (Fig. 3). Cooling probes were targeted to the dorsomedial side of Uva. (A) Sagittal section. (B) Coronal section. . **C**, Modified Peltier cooling device with extended heat sink. **D**, Schematic showing the positions of the cooling probe and the extended heat sink. **E**, an example of HVC temperature during Uva cooling with and without extended heat sink. **F**, Relationships between the temperature near Uva and HVC. **G,** Decay of temperature changes measured at various depths when the surface of HVC is cooled (black circles) or when thalamic regions near Uva are cooled (blue circles).

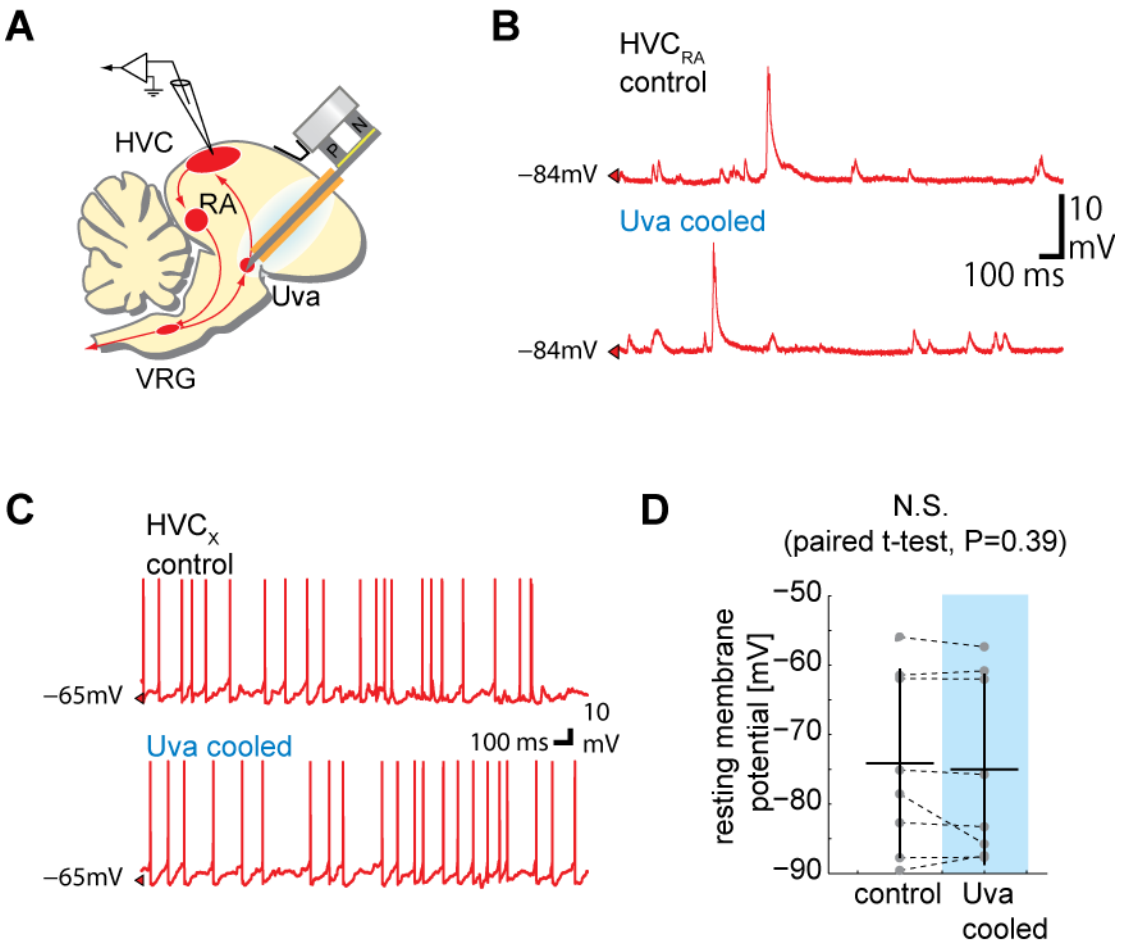

Figure S5 (related to Figure 5) | Uva cooling does not affect resting membrane potentials of HVC neurons. A, Schematic diagrams of the experiments. After measuring the song dilation effect of Uva cooling, a subset of birds of which HVC temperature were well clamped were used for sharp intracellular recordings from HVC neurons under isoflurane anesthesia. **B**, **C**, example traces of membrane potential dynamics of HVC_{RA} (B) and HVC_x (C). **D**, Uva cooling did not change the resting potential of HVC PNs (n = 3 HVC_{RA}, n = 3 HVC_X, n = 2 $HVC_{int,}$ $P < 0.39$).

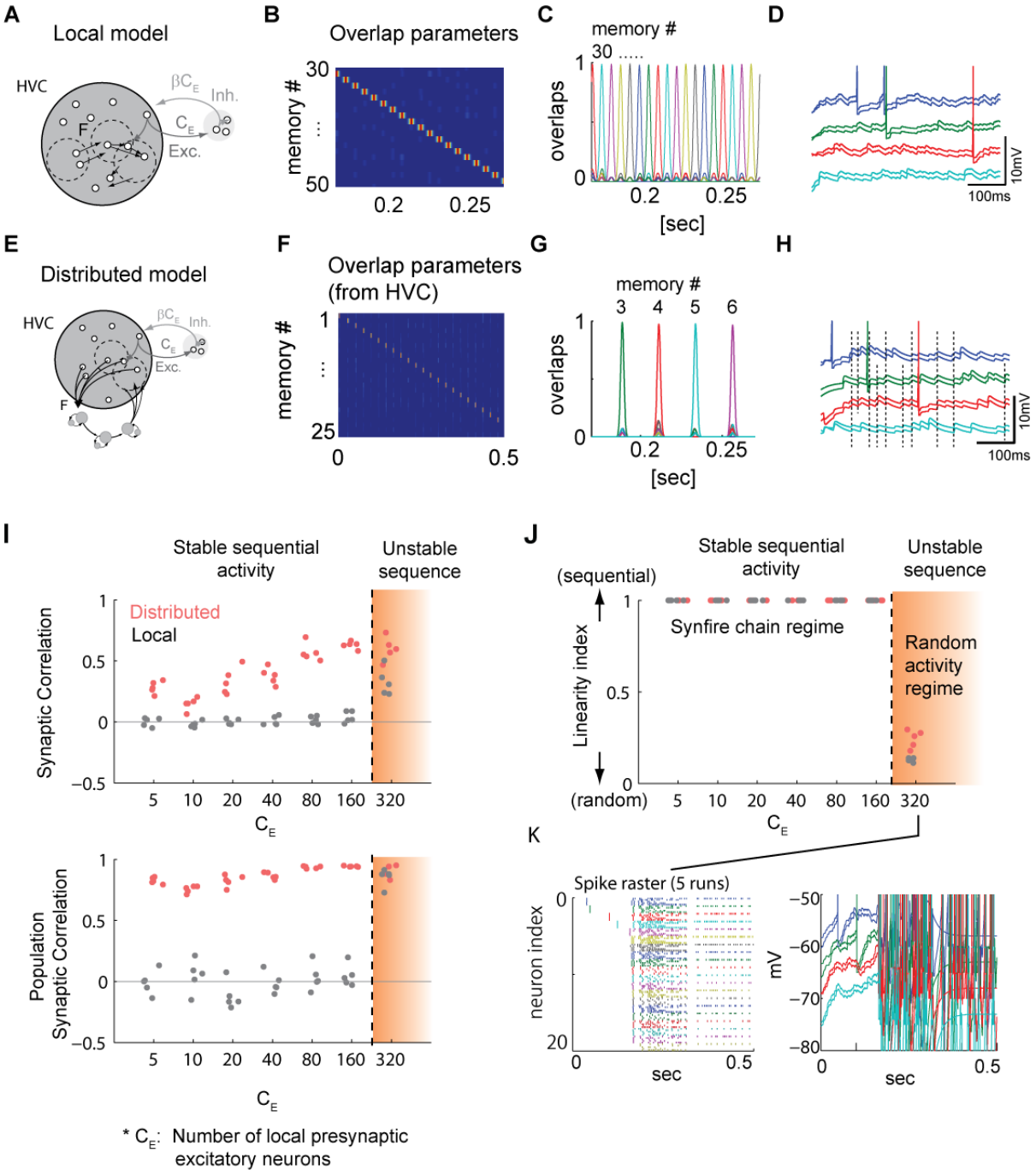

Figure S6 (related to Figure 6) | (Simulation Result) Overlap parameters and membrane potential dynamics in two models. **A,** Schematic of local chain models. **B**, Overlap parameters represent the similarity between the action potential activity and each memorized pattern. The sequential activation pattern of overlap parameters indicates that the embedded patterns are activated in the correct order. **C,** When one of the overlap parameter is activated, the activity of some of other overlap parameters is slightly elevated (small fluctuations near the baseline) due to the divergent connections. This indicates that a small number of cells are activated outside of the correct timing; however, these numbers are not large enough to disturb the correct flow of the activation pattern. **D,** Examples of membrane potential traces from two runs of simulations in the local model. **E,** Schematic of distributed chain models. **F**,**G**,

Overlap parameter plots of HVC neurons in distributed chain models. **H**, Examples of membrane potential traces from two runs of simulations in the distributed model. **I**, Synaptic correlation from pairs (Top) and populations (Bottom) of neurons with various numbers of local recurrent excitatory connections, C_E. Each dot is calculated from 5 runs of simulations in the same network with different initial conditions in membrane potential values. Within the chain network regime ($C_E < 320$), the distributed but not the local chain models generate correlated synaptic activity. **J**, As the number of local interactions C_E increases, sequential activity is no longer maintained (orange shaded region), and the network dynamics approaches the random activity regime in which random action potential activity is maintained by local random connections. **K**, An example of network activity (left) and membrane potential dynamics (right) near the boundary of synfire chain and random activity regimes ($C_E = 320$, Local chain model).

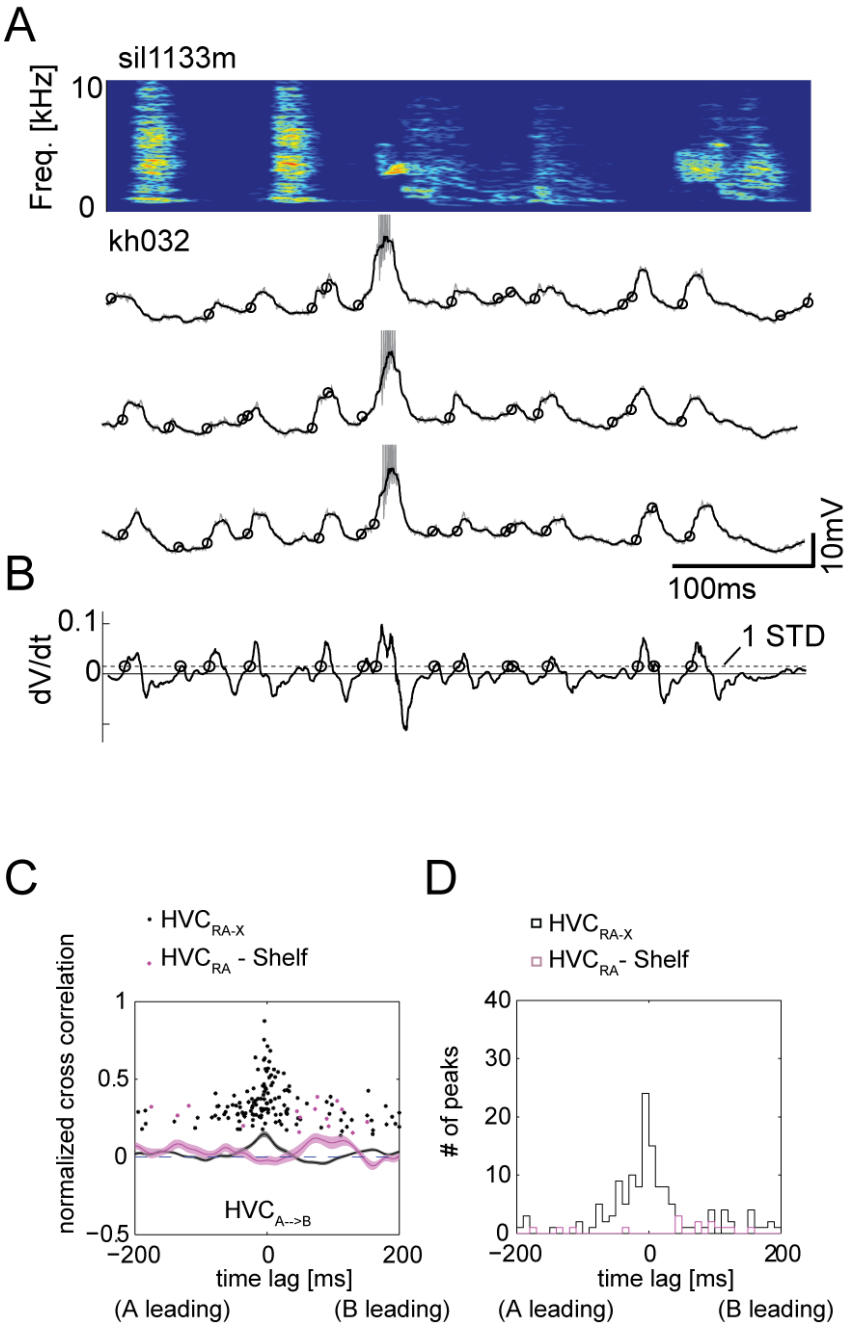

Figure S7 (Related to Figure 8)| dPSP detection algorithm can detect most large depolarizing synaptic events. The synaptic onset timings of HVC_{RA} and HVC_X neurons are not significantly biased from time lag zero. A, Examples of HVC_{RA} cells membrane potential dynamics during singing (grey lines) and median filtered traces (5ms window, black lines). Circles: detected dPSP onsets. **B,** An example of d*V*/d*t* trace measured from the bottom trace in (A). The detection threshold is 1xSTD of d*V*/d*t* trace. **C**, Normalized cross correlation of synaptic onset timing between HVC_{RA} - HVC_X (black) and HVC_{RA} – Shelf (red) neuron pairs. The peaks of cross correlation values of all the pairs are plotted. Population averaged synaptic correlation is plotted with SEM (hatched region). **D**, The distribution of the peak timings for HVC_{RA} - HVC_X pairs and HVC_{RA} - Shelf pairs.

References for Supporting Information

Brunel, N. (2000). Dynamics of Sparsely Connected Networks of Excitatory and Inhibitory Spiking Neurons. J Comp Neurosci *8*, 183-208.

Hahnloser, R.H., Kozhevnikov, A.A., and Fee, M.S. (2002). An ultra-sparse code underlies the generation of neural sequences in a songbird. Nature *419*, 65-70.

Ishibashi, K., Hamaguchi, K., and Okada, M. (2006). Theory of Interaction of Memory Patterns in Layered Associative Networks. Journal of the Physical Society of Japan (JPSJ) *75*, 114803.

Long, M.A., and Fee, M.S. (2008). Using temperature to analyse temporal dynamics in the songbird motor pathway. Nature *456*, 189-194.

Long, M.A., Jin, D.Z., and Fee, M.S. (2010). Support for a synaptic chain model of neuronal sequence generation. Nature *468*, 394-399.

Mooney, R., and Prather, J.F. (2005). The HVC Microcircuit: The Synaptic Basis for Interactions between Song Motor and Vocal Plasticity Pathways. J Neurosci *25*, 1952-1964.

Scharff, C., Kirn, J.R., Grossman, M., Macklis, J.D., and Nottebohm, F. (2000). Targeted neuronal death affects neuronal replacement and vocal behavior in adult songbirds. Neuron *25*, 481-492.